

Stochastic Multiscale Characterization of Short-Fiber Reinforced Composites

M.A. Hickman, P.K. Basu

A framework for stochastic modelling and optimization of materials with engineered microstructures is presented. Numerical methods for solving problems with short-fiber inclusions are discussed. Addition of fiber reinforcement has been shown to improve the performance of various materials in a number of applications. The response of fiber reinforced concrete under tensile stress is dependent upon several properties, including fiber geometry, fiber material properties, fiber length, and orientation of the fibers with respect to the applied load. In a real-world system the distribution of the fibers may be random, with orientation angle and configuration varying locally. Stochastic multiscale methods enable the connection of the scales to analyze the effect of randomly distributed short-fiber inclusions on the global response of the system. Randomly generated characteristic volume elements (CVE) are analyzed using the extended finite element method (XFEM) to capture local material response without the need for a mesh that conforms to the material morphology, ideal for situations with arbitrary fiber distributions. The variation observed in statistically equivalent CVE models is quantified. Correlation is determined between FRC descriptor variables and the tensile response of the composite. It is demonstrated that machine learning can be used to predict composite material properties of FRC to a reasonable degree of accuracy using information about the material microstructure.

1 Introduction

All physical systems, natural and engineered, are characterized by some degree of inherent uncertainty. Uncertainty is present on all scales, from the atomic arrangement of a material microstructure, to the demand imposed on the system at the macroscale. Design of materials with engineered microstructures requires characterization of this uncertainty to assess the reliability of the material performance in expected scenarios so that the design life of the structure can be predicted. Multiscale modelling allows for the bridging of uncertainty across spatial and temporal scales and has become a useful tool in several engineering and science disciplines where materials with heterogeneous microstructures are commonly used. The purpose of this research is to develop a computational framework for the design of composite material microstructures to optimize the desired structural performance of a fiber reinforced composite (FRC). This will enable intelligent tailoring of a mix of material phases of different types, shapes, and sizes satisfying the needs of a particular application in terms of performance, cost, and ease of manufacture.

The current emphasis on rational performance driven design approaches (Li and Fischer, 2002) requires a more critical look towards realizing the desired material performance by closer link of material constituents with structural performance. For instance, in the case of short-fiber reinforced composites, apart from the strength of the matrix material, its ductile performance can be a factor of volume percentage, diameter, strength, length, distribution, elastic modulus, and, most importantly, the interfacial mechanical and chemical bond characteristics of the two. Li (1992) proposes a hierarchical design method in which optimal microstructure processing techniques and characteristics are identified to achieve a target structural response. Fundamental to the approach is identification of a quantitative relationship between microstructure composition and material response. At the microstructure level, we are concerned with how morphology, processing, and optimization techniques influence material properties. The large-scale performance is dependent on the interaction between material properties, the environment, and the geometry of the structural element.

In order to accurately predict the response of an object at the macroscale, it is necessary to consider the localized behavior of component phases and interactions between them in the meso- or smaller scale. In the case of heterogeneous materials like ceramics and concrete, there is a significant degree of uncertainty in connecting the scales,

creating complexities in the characterization of the material at all the scales of interest. The physical response of such materials is controlled by the mechanical characteristics of the constituent phases. Historically these materials have been characterized on the basis of strength tests, resulting in a number of empirical relationships that have been used by engineers. Such test-based empirical characterization methods may be a viable option for relatively inexpensive materials but the design of new-age composites can be time consuming and expensive tests may not be an acceptable option.

This paper aims to draw a connection between characteristics of FRC on the mesoscale and material properties that govern performance at the structural scale. In addition to morphological heterogeneity, the effect of interaction between constituent materials is considered. Section 2 reviews approaches to multiscale modelling of FRC and proposes a sequential multiscale modelling framework. Section 3 describes the large-scale, homogenized behavior of a brittle-matrix composite reinforced by ductile fibers and the manner in which a plasticity model is capable of computationally modelling the associated physical phenomena. Section 4 provides a brief overview of the extended finite element method (XFEM) and its ability to efficiently model the interaction between the matrix and fibers at the mesoscale. Section 5 overviews the exploration of design space and numerical model parameters. Sections 6 and 7 consider the model results and comment on the viability.

2 Stochastic Multiscale Modelling Approach

The inelastic response of FRC is controlled primarily by interaction between fiber and matrix, leading to post-peak strain-softening when the matrix cracks. The material properties of each phase, aspect ratio of inclusions, and volume content have all been shown to influence the behavior of the composite, among other factors. An engineered FRC at the structural scale (10^{-1} - 10^0 m) may contain thousands of short fibers ($\sim 10^{-3}$ m in length). As it is impractical to explicitly discretize every single fiber in the problem domain, homogenized strength properties are often used for the macroscale model, under the assumption that fibers are uniformly distributed. However, in an engineered composite with randomly distributed fibers, their orientation angle and distribution vary with location. In a large problem domain, local heterogeneity may be observed, introducing uncertainty in the performance of the system across scales. Figure 1 shows a domain containing randomly distributed fibers with a prescribed volume fraction of 0.1%. A division of this domain into four subdomains shows that the volume fraction observed in each subdomain appears to differ significantly from the average for the global domain with a minimum of 0.047% and a maximum value of 0.141%. This study proposes a stochastic multiscale method to connect the scales such that the effect of randomly distributed inclusions on the global response of the system can be accounted for. At the macro level a plasticity model of the composite is considered, neglecting the presence of individual fibers due to their small length with respect to the size of the global problem domain. The presence of fibers is accounted for by analyzing random realizations of mesoscale composites using XFEM and characterizing the nonlinear relationship between morphology and material properties.

Representative volume elements (RVE) are used extensively in structural mechanics in the context of multiscale modelling of composite materials. A RVE is defined as, “a volume of heterogeneous material that is sufficiently large to be statistically representative of the composite” (Kanit et al., 2003). The RVE approach sometimes assumes periodicity in the material composition at a small scale, which can be coupled with a homogenization tool. Yuan et al. (1997) assessed the effect of fiber-matrix interfacial debonding and fiber orientation on elastic response of a composite using a finite element model for the RVE. Kabele (2007) analyzed RVE response in the context of integrated structures and material design using the finite element method and spatial averaging to connect scales in a sequential approach. The finite element method (FEM) is commonly used to model fiber-matrix debonding at the mesoscale using cohesive elements at the interfacial phase boundary. However, conventional FEM is ill-suited to handle complex microstructure geometries due to the need to explicitly mesh the domain (a problem discussed further in Section 4). XFEM has emerged as an efficient alternative to cohesive zone modelling, and its usefulness has been demonstrated for woven reinforcement (Kastner et al., 2013) and random short-fiber reinforcement (Pike and Oskay, 2015b).

Unique challenges arise in identifying the RVE of a material with randomly distributed inclusions, requiring special treatment from a multiscale modelling perspective. Previous studies have used a descriptor-based approach to characterize the behavior of heterogeneous cementitious materials containing voids on the microscale (Xu et al., 2014). In the descriptor-based approach, a correlation is assumed between variables that describe the material on the microscale, called descriptors, and measurable material parameters. The descriptors detail the shapes and spatial alignment of inclusions, aspect ratios, and volume fractions of each material phase in the matrix, and are mapped to material parameters by Kriging. Identification of descriptors provides a challenge in reducing the design

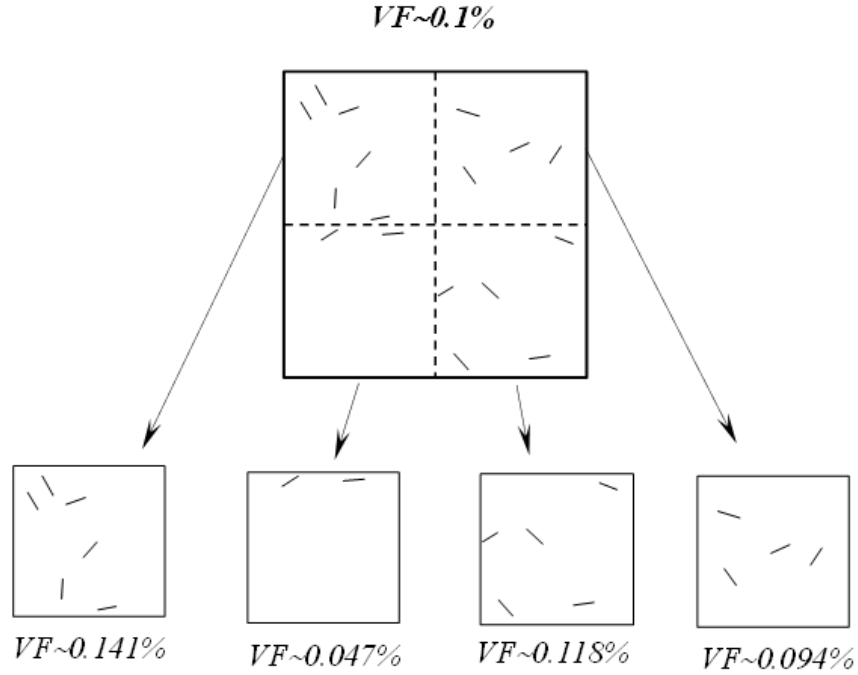


Figure 1. Local variation of fiber volume content

space into a finite number of dimensions. Use of too many dimensions creates a complex regression problem. Clement et al. (2013) demonstrated the use of polynomial chaos expansion to account for a high number of random variables inherent in the characterization of randomly heterogeneous media. Xu et al. (2013) decomposed random RVEs containing elliptical inclusions into smaller statistical volume elements (SVE) whose response was analyzed and quantified for upscaling. The approach is similar to that used by Ghosh et al. (2007), who uses a statistically equivalent RVE (seRVE) to model FRC at the microscale within the context of a concurrent multiscale model using Voronoi cell FEM. Greene et al. (2013) identifies scenarios where uncertainties significantly affect macroscale behavior using a statistical description of microstructure for three benchmark problems. Clement et al. (2012) developed a database of elementary cells of fiber reinforced polymers containing arbitrary heterogeneities within the stochastic dimension. One useful aspect of the research is that different microstructures may continue to be modelled and added to the database, which can be used within a hierarchical multiscale framework. In general, multiscale methods are classified as hierarchical or concurrent. Concurrent models solve systems of different scales in parallel, passing information between the models used at each scale. In the process, the macroscale response is influenced by the microscale response, and vice-versa. In a hierarchical model, however, averaging is used to connect the scales, and simulations at each scale are performed sequentially.

In this work a hierarchical multiscale modelling approach is presented for random FRC so that the effects of interaction of individual fibers may be analyzed at the mesoscale using a suitable modelling tool (XFEM). A database relating material composition to composite response is developed. The observed composite properties may then be passed to the macroscale, where a homogenized plasticity model can be used with stochastic finite elements to assess the large-scale performance of the random composite in an efficient and convenient manner. A schematic of the approach is shown in Figure 2. The method consists of four steps: (1) stochastic sample generation, (2) mesoscale modelling and characterization, (3) homogenization, and (4) design sensitivity analysis (macroscale modelling). In step 1, descriptor variables are selected to quantify microstructure characteristics that are assumed to influence material properties. Points in descriptor space are sampled and used to generate random microstructures with a range of design values. The selection of descriptors and sampling technique are discussed in Section 5. The random samples are analyzed using XFEM in step 2. Gaussian process (GP) regression is used to quantify the multivariate nonlinear relationship between descriptors and measured material properties. Optimal microstructure designs can be selected based on their measured performance. In step 3, the GP is used to predict properties of subdomains in a macroscale model that correspond to unknown points in the descriptor space. At the macroscale, the material is modelled as homogeneous with each subdomain described by unique material properties. Fiber randomness effects are accounted for by locally prescribed variations in composite material response rather than modelling fiber-matrix interaction effects. This enables the reliability of a macro structure to be assessed, taking into account the local randomness of design variables (step 4). This work focuses primarily on

steps 1-2. Future work will address homogenization and design reliability assessment at the macroscale.

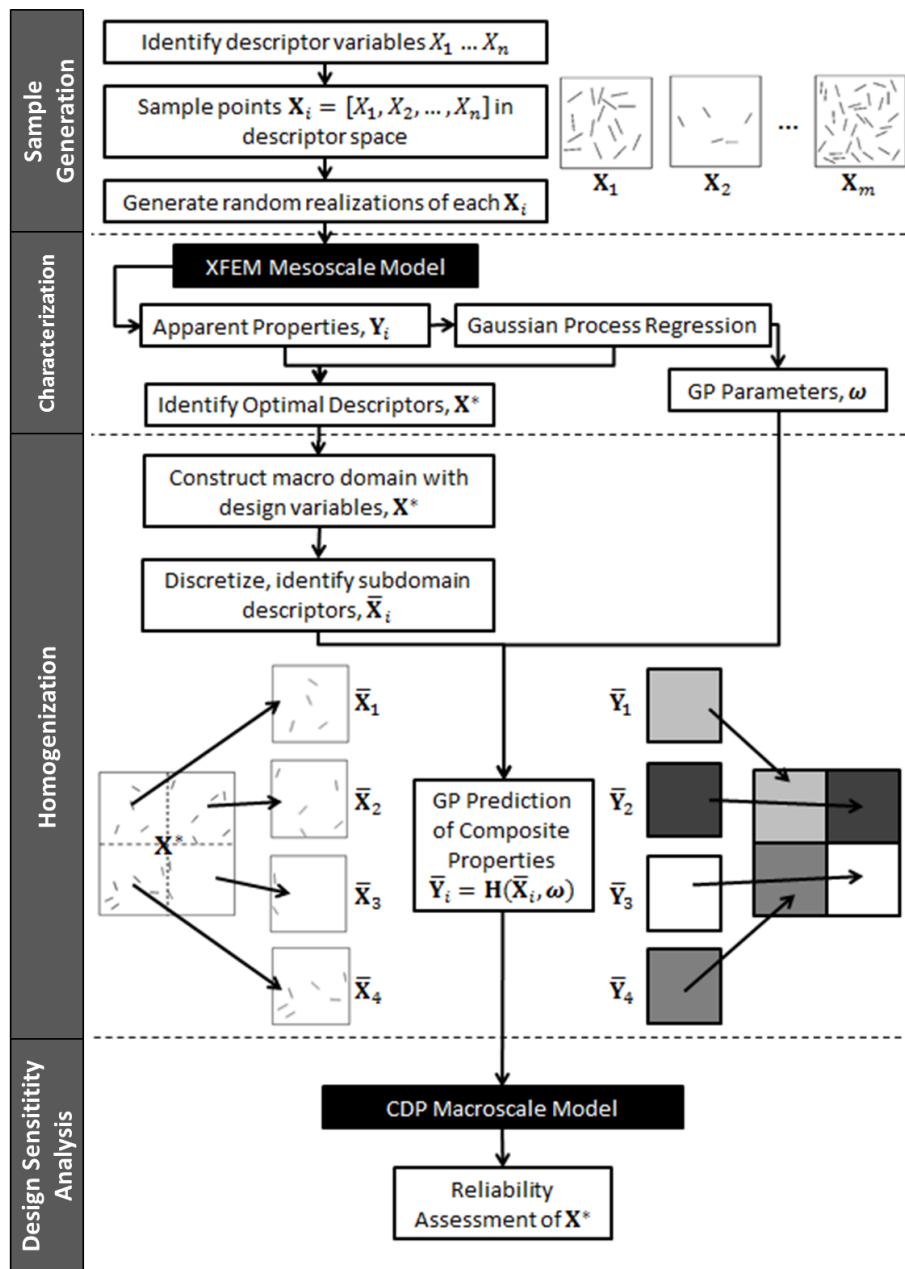


Figure 2. Sequential multiscale modelling framework for FRC

3 Mechanical Behavior of FRC

In a cementitious FRC, the matrix material is characterized by high compressive strength and relatively low tensile strength, which is often compensated for in the design through the addition of suitable reinforcement. In traditional design, such reinforcement is typically aligned to withstand a load with some prescribed orientation. More recently, short fibers have been used to provide improvement in the tensile response and ductility in a number of applications. The reinforcement provides crack bridging, extra ductility, and energy absorption capability without significantly increasing the weight of the composite (Bentur and Mindess, 1990). In cases where the orientation of the load with respect to the reinforcement is variable, randomly distributed fiber reinforcement can be used to enable effectively isotropic material behavior. The behavior of FRC under tensile stress is dependent on several properties, including fiber aspect ratio, fiber and matrix stiffnesses, and inclusion volume content. Random FRC can be fabricated more easily than composites with aligned reinforcement, but poses challenges in property characterization. Figure 3 depicts 6 FRC microstructures randomly generated using the same input parameters for fiber



Figure 3. Random microstructure realizations with volume fraction = 0.1%, Fiber Length = 3.27 mm

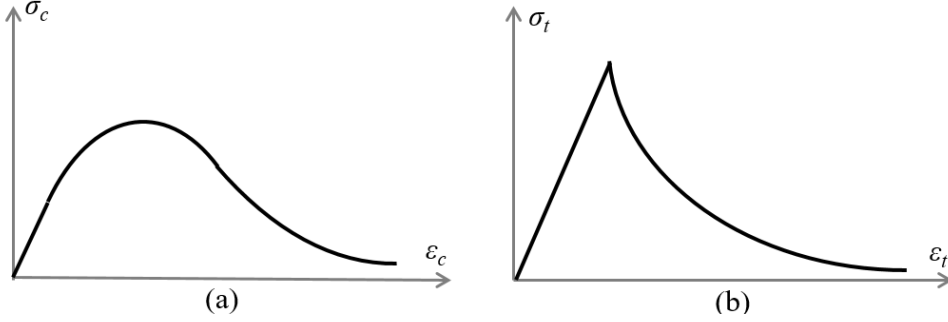


Figure 4. Common FRC behavior in uniaxial compression (a) and tension (b)

length and volume fraction. It can be clearly observed that significant variation in the fiber concentration exists despite using equivalent design values.

Figure 4 shows typical stress-strain curves for a brittle matrix FRC under uniaxial compression and tension. The compressive response of FRC does not differ significantly from the unreinforced matrix. The matrix carries the bulk of the imposed load and the inelastic response is dictated by crushing and filling of voids in the microstructure. This study focuses primarily on the tensile response of the composite, which is influenced largely by the fibers in the matrix. Following an initial linear elastic range, the brittle matrix cracks and the load is transmitted to fibers through cohesive bonds, which results in post-peak softening, as shown.

3.1 Macroscale Damage-Plasticity Model for Homogenized FRC

A number of approaches exist for modelling the homogenized behavior of FRC. Lubliner et al. (1989) presented a constitutive model capable of accurately predicting the nonlinear, multiaxial behavior of concrete using plasticity theory. The model is commonly known today as the Concrete Damage Plasticity (CDP) model, and can be easily and efficiently implemented using commercial finite element analysis software such as Abaqus. The model consists of a yield criterion, a hardening rule, and a flow rule that can be fully defined by four parameters calibrated to uniaxial tension, uniaxial compression, biaxial compression, and triaxial compression tests. The CDP model is an attractive macroscale model for FRC due to its independent definition of tensile and compressive stiffness degradation. For a given state of strain, the resulting tensile stress is interpolated from the data.

Jankowiak and Lodygowski (2005) provides a detailed description of the parameter calibration process using experimental results. A brief overview of the CDP model is given here for the sake of completeness. The CDP constitutive equation is given by equation (1).

$$\bar{\sigma} = \mathbf{D}_0^{el}(\boldsymbol{\varepsilon} - \boldsymbol{\varepsilon}^{pl}) \in \{\bar{\sigma} | F(\bar{\sigma}, \bar{\boldsymbol{\varepsilon}}^{pl}, f, K_c) \leq 0\} \quad (1)$$

where $\bar{\sigma}$ is the effective stress, defined in terms of total strain $\boldsymbol{\varepsilon}$, plastic strain $\boldsymbol{\varepsilon}^{pl}$, and initial elasticity matrix \mathbf{D}_0^{el} . F is the yield surface with parameters f , the ratio of the biaxial compressive strength to the uniaxial compressive strength, and K_c , the ratio of the second stress invariant on the tensile meridian to the second stress invariant on the compressive meridian, which shapes the deviatoric load surface. The effective stress is related to the Cauchy stress tensor $\boldsymbol{\sigma}$ by equation (2).

$$\boldsymbol{\sigma} = [1 - d(\bar{\boldsymbol{\varepsilon}}^{pl})] \bar{\boldsymbol{\sigma}} \quad (2)$$

where $d(\bar{\boldsymbol{\varepsilon}}^{pl})$ is the scalar damage variable. $\bar{\boldsymbol{\varepsilon}}^{pl} = [\bar{\varepsilon}_c^{pl} \quad \bar{\varepsilon}_t^{pl}]^T$ is the hardening variable, with components corresponding to compression and tension. The value of the hardening variable is non-decreasing and taken as

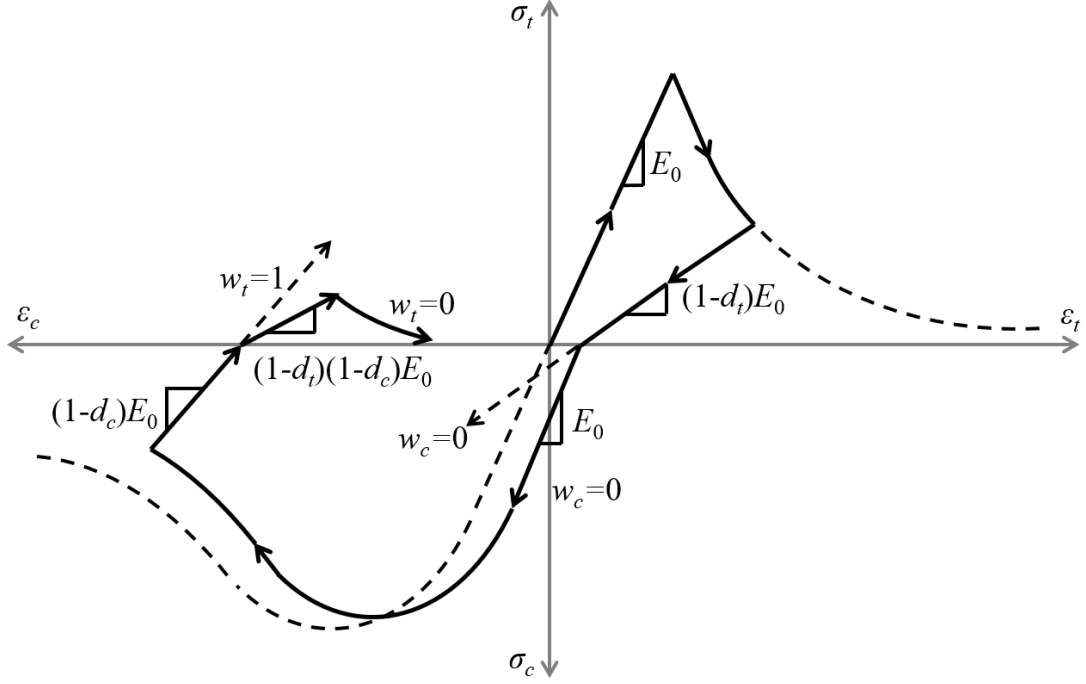


Figure 5. Effect of stiffness recovery factors on load-reversal response

$\tilde{\epsilon}^{pl} = \int_0^t \dot{\tilde{\epsilon}}^{pl} dt$. The evolution of the hardening variable is given by equation (3).

$$\dot{\tilde{\epsilon}}^{pl} = \begin{bmatrix} \dot{\tilde{\epsilon}}_t^{pl} \\ \dot{\tilde{\epsilon}}_c^{pl} \end{bmatrix} = \begin{bmatrix} r(\hat{\sigma}) \dot{\tilde{\epsilon}}_{max}^{pl} \\ -[1 - r(\hat{\sigma})] \dot{\tilde{\epsilon}}_{min}^{pl} \end{bmatrix} \quad (3)$$

here $r(\hat{\sigma})$ is a stress weight factor for the multiaxial case that is dependent upon the principal effective stresses, $\hat{\sigma}$. $\dot{\tilde{\epsilon}}_{max}^{pl}$ and $\dot{\tilde{\epsilon}}_{min}^{pl}$ are the maximum and minimum eigenvalues of the plastic strain rate tensor. Equation (4) defines the stress weight factor.

$$r(\hat{\sigma}) = \frac{\sum_{i=1}^3 \langle \hat{\sigma}_i \rangle}{\sum_{i=1}^3 |\hat{\sigma}_i|} \quad (4)$$

$\langle \cdot \rangle = ((\cdot) + |\cdot|)/2$ represents the Macaulay brackets. The stress weight factor is equal to 1 for pure tension and 0 for pure compression. The scalar damage variable $d(\tilde{\epsilon}^{pl})$ is a function of the user-defined uniaxial damage variables $d_t(\tilde{\epsilon}_t^{pl})$ and $d_c(\tilde{\epsilon}_c^{pl})$. For multiaxial stress it is assumed that the damage variable can be calculated using equation (5).

$$d = 1 - (1 - s_t d_c)(1 - s_c d_t) \quad (5)$$

Computed parameters s_t and s_c are introduced to incorporate stiffness recovery effects into the model. Equation (6) gives the expression for the stiffness recovery parameters.

$$\begin{bmatrix} s_t \\ s_c \end{bmatrix} = \begin{bmatrix} 1 - w_t r(\hat{\sigma}) \\ 1 - w_c [1 - r(\hat{\sigma})] \end{bmatrix} \quad (6)$$

The parameters w_t and w_c dictate whether stiffness is recovered when loading changes from tension to compression. In general, quasi-brittle materials show compressive stiffness recovery when cracks open in tension and close in compression, but no stiffness is recovered in tension following initiation of cracking. This effect is captured by setting $w_t = 0$ and $w_c = 1$. The influence of the damage variables and recovery parameters on material stiffness are summarized in Figure 5. The non-associative flow rule is given by equation (7).

$$\dot{\tilde{\epsilon}}^{pl} = \dot{\lambda} \frac{\partial G(\bar{\sigma}, \psi, \epsilon)}{\partial \bar{\sigma}} \quad (7)$$

Here $\dot{\lambda}$ is the non-negative plastic multiplier and ψ and ϵ are parameters that shape the flow surface, referred to as the dilation angle and eccentricity, respectively. G is the scalar-valued flow potential function, given by the

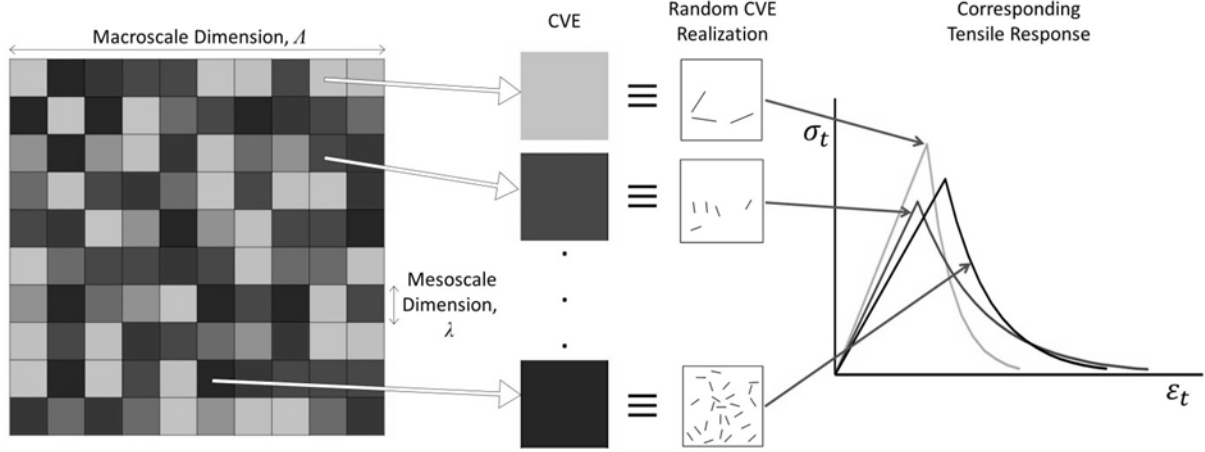


Figure 6. Homogenization approach for capturing local variation in tensile response

Drucker-Prager hyperbolic function in equation (8).

$$G(\bar{\boldsymbol{\sigma}}, \psi, \epsilon) = \sqrt{(\epsilon \tan \psi)^2 + \bar{q}^2} - \bar{p} \tan \psi \quad (8)$$

$\bar{p} = -\frac{1}{3}I_1$ is the effective hydrostatic pressure with I_1 representing the first invariant of the effective stress tensor and $\bar{q} = \sqrt{\frac{3}{2}\bar{\mathbf{S}} : \bar{\mathbf{S}}}$ is the Mises equivalent effective stress, defined in terms of the deviatoric effective stress $\bar{\mathbf{S}} = \bar{p}\mathbf{I} + \bar{\boldsymbol{\sigma}}$. Since $\dot{\lambda} = 0$ when $F < 0$ and $\dot{\lambda} > 0$ when $F = 0$, the Kuhn-Tucker condition is given by $\dot{\lambda}F = 0$. The consistency condition $\dot{F} = 0$ follows from the assumption that when plastic slip is occurring the state of stress remains on the yield surface.

3.2 Accounting for Local Fiber Randomness at the Macroscale

The effect of reinforcement on the tensile response of the composite is included directly into the model using data from the uniaxial tension test. Due to random local variation of fiber content within a structure, it is not convenient to use the same strain softening curve to define tensile behavior throughout the global problem domain. Figure 6 illustrates an alternative approach to homogenization. Here, a domain of length scale Λ is discretized into subdomains of scale λ , called characteristic volume elements (CVE). Each CVE is assigned a unique tensile stress-strain relationship based on its morphology. CVEs with statistically equivalent properties (say, volume fraction, fiber length, etc.) can be characterized by similar material properties. Statistically equivalent CVEs are identified by identical shades, as shown in Figure 6. It should be noted that there is no pattern to the occurrence of statistically equivalent CVEs, which follows from the lack of periodicity in the material. The determination of parameters for each CVE is carried out using XFEM, as detailed in Section 4.

For characterization of the composite response, the behavior of FRC in tension is idealized by the following 4-parameter piecewise equation.

$$\sigma_t(\epsilon_t) = \begin{cases} \left(\frac{\sigma_i}{\epsilon_i}\right)\epsilon_t & \forall \epsilon_t \in [0, \epsilon_i] \\ \sigma_i e^{-\alpha(\epsilon_t - \epsilon_i)} & \forall \epsilon_t \in [\epsilon_i, \epsilon_f] \end{cases} \quad (9)$$

The equation consists of an initial elastic region followed by an exponentially decaying post-peak softening region. Here σ_i is the peak stress at which the concrete matrix cracks and the fibers are engaged and ϵ_i is the strain corresponding to σ_i . ϵ_f is the strain at which the composite fails. α is an exponential decay parameter that controls the shape of the post peak softening region, as depicted in Figure 4a. ϵ_t and σ_t are the experimentally determined stress vs. strain data to which the equation must be fit. The failure strain of the composite, ϵ_f , is defined as the strain at which the tensile stress has degraded to 10% of the peak value. Fiber plasticity and fracture are not considered here but may be included in future studies. The area under the stress-strain curve represents the total strain energy capacity of the material in tension, known as the modulus of toughness, G^t . The area under the linear elastic region of the curve is known as the modulus of resilience, denoted by G^r , defined as the amount of energy that can be absorbed by the material prior to inelastic deformation. The modulus of resilience is calculated using

equation (10).

$$G^r = \int_0^{\varepsilon_i} \left(\frac{\sigma_i}{\varepsilon_i} \right) \varepsilon_t d\varepsilon_t = \frac{1}{2} \sigma_i \varepsilon_i \quad (10)$$

The modulus of toughness is obtained by summing the modulus of resilience with the area under the post-peak region of the stress-strain curve as given by equation (11).

$$G^t = G^r + \int_{\varepsilon_i}^{\varepsilon_f} \sigma_i e^{-\alpha(\varepsilon_t - \varepsilon_i)} d\varepsilon_t \quad (11)$$

For homogenization, the measured strain energy is converted to strain energy density by normalizing over the CVE volume. By equating the energy density across scales, the Hill-Mandel macrohomogeneity condition is satisfied. CVE size effect is for now being deferred to future effort.

4 XFEM Approach to Mesoscale Modelling

XFEM has been tailored for a variety of problems in material analysis and design. The approach can be used to model fracture, dislocations, grain boundaries, and phase interfaces. Belytschko and Gracie (2009) provided a comprehensive review of the constantly evolving state-of-the-art of XFEM. The method has been extensively used to model cracks and inclusions within multiphase materials. Recently, Kastner et al. (2013) used XFEM to capture the inelastic response of textile-reinforced polymers. Savvas et al. (2014) stochastically analyzed the effect of elliptical inclusion aspect ratio on elastic behavior. Daux et al. (2000) proposed a method for handling multiple discontinuities within an element, where cracks propagate and eventually form a junction. Zi et al. (2004) demonstrate that the junction of two cracks can be handled more easily by combining two step enrichments rather than using a special enrichment function for the junction. Modelling multiple fibers in an element requires superposition of enrichment functions, and characterization of interaction effects. Hiriyur et al. (2011) proposed a displacement approximation for elements containing multiple inclusions.

XFEM uses standard finite element shape functions to approximate the displacement field, along with enrichment functions to capture the local variation of the displacement field due to the presence of discontinuities in the material. The local enrichment functions are selected a priori according to the nature of the problem and satisfy the partition of unity, so that the local enrichment does not affect the global solution. The general form of the XFEM approximation field is given as

$$\mathbf{u}(\mathbf{x}) = \sum_{a=1}^{n_n} \mathbf{N}_a(\mathbf{x}) \mathbf{u}_a + \sum_{b \in I} \mathbf{N}_b(\mathbf{x}) \psi_b(\mathbf{x}) \mathbf{v}_b \quad (12)$$

\mathbf{u} is the displacement; $\mathbf{N}_a(\mathbf{x})$ the shape function of node a ; $\psi_b(\mathbf{x})$ is the enrichment function for the inclusion at node b in set I , the index set of enriched nodes; \mathbf{u}_a and \mathbf{v}_b are the nodal coefficients of the standard nodes and the fiber enrichment shape functions. n_n is the number of nodes in the problem domain. Level-set methods make it possible to determine unique enrichment functions for an arbitrarily oriented inclusion within a finite element. Weakly discontinuous enrichment functions can capture the strain discontinuity in an element, whereas a strongly discontinuous function can capture discontinuity in the displacement field.

4.1 XFEM for Random FRC with Cohesive Debonding

Pike and Oskay (2015a) presented an approach for modelling the behavior of a matrix containing stretchable short-fiber inclusions using XFEM. The enrichment functions were derived to model the strain discontinuity resulting in an element due to an arbitrarily placed high aspect ratio fiber. More recently, the XFEM model was improved to include the effect of cohesive debonding between the matrix and inclusions. An additional enrichment function was derived to model the displacement discontinuity in an element as a result of debonding (Pike and Oskay, 2015b). A nonlocal damage model was used to capture the stiffness degradation of the matrix material. The authors demonstrated that with sufficient mesh refinement XFEM is capable of accurately reproducing the local mechanical response observed in a reference FEM model. The primary advantage of using XFEM for random FRC modelling is that the mesh does not need to conform to the morphology of the problem domain. Depending upon the arrangement of the inclusions, the standard FEM mesh may be geometrically complex and require an unreasonably large number of elements to accurately solve the problem. The XFEM problem formulation and enrichment function derivation is outside the scope of this paper, but is discussed briefly in this section to provide

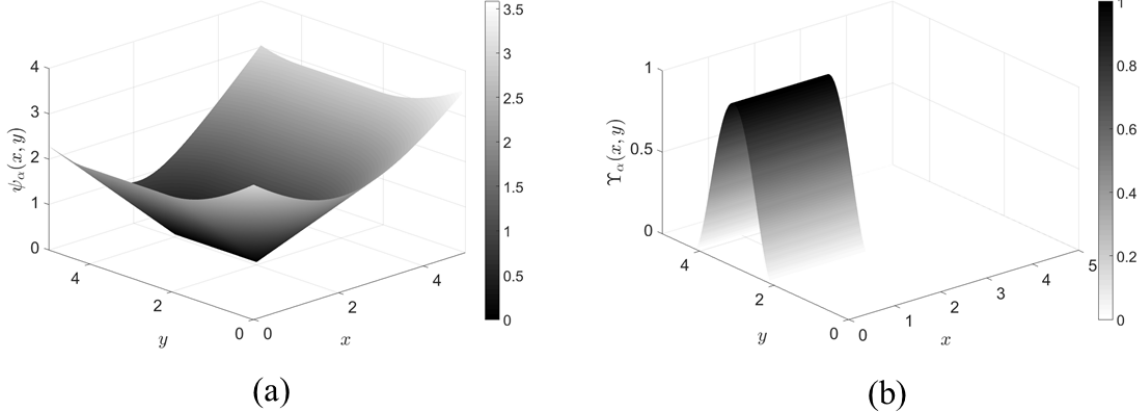


Figure 7. Visualization of enrichment functions for an arbitrarily placed fiber in a 5x5 element domain: (a) strain discontinuity enrichment function; and (b) debonding enrichment function

a broad overview of the numerical method used for mesoscale analysis in the proposed multiscale modelling approach. The approximation of the displacement field is given by equation (13).

$$\mathbf{u}(\mathbf{x}) = \sum_{a=1}^{n_n} \mathbf{N}_a(\mathbf{x}) \mathbf{u}_a + \sum_{\alpha=1}^n \left[\sum_{b=1}^{n_{en}^\alpha} \mathbf{N}_{\mathcal{I}_b^\alpha}(\mathbf{x}) \psi_\alpha(\mathbf{x}) \mathbf{v}_{b\alpha} \right] + \sum_{\alpha=1}^n \left[\sum_{c=1}^{n_{en}^\alpha} \mathbf{N}_{\mathcal{I}_c^\alpha}(\mathbf{x}) \Upsilon_\alpha(\mathbf{x}) \mathbf{w}_{c\alpha} \right] \quad (13)$$

The formulation is similar to equation (12) but contains an additional enrichment function $\Upsilon(\mathbf{x})$ to capture the debonding along the fiber-matrix interface, while $\psi(\mathbf{x})$ captures the discontinuity in the strain field. The enrichment functions depend on the location of fiber α within the domain. n is the number of fibers in the domain, and n_{en}^α is the number of nodes enriched by fiber α . \mathbf{u}_a , $\mathbf{v}_{b\alpha}$, and $\mathbf{w}_{c\alpha}$ are the nodal coefficients of the standard nodes, fiber motion enrichment, and debonding enrichment shape functions.

The fibers are assumed lie entirely within the domain of the composite. The high aspect ratio fiber is idealized as a line segment within the domain and is defined using the level set functions ϕ_c and ϕ_λ .

$$\phi_c(\mathbf{x}) = \|\mathbf{x} - \mathcal{P}(\mathbf{x})\| \quad (14)$$

$$\phi_\lambda(\mathbf{x}) = (\mathbf{x} - \mathbf{x}_\lambda) \cdot \mathbf{t}_\lambda; \quad \lambda = 1, 2 \quad (15)$$

ϕ_c is equal to 0 along the fiber line segment and takes positive values on either side of the fiber. ϕ_λ is the level set function for the two fiber tips ($\lambda = 1, 2$). $\mathcal{P}(\mathbf{x})$ is the projection of \mathbf{x} onto the fiber. \mathbf{x}_λ is the position of the fiber tip and \mathbf{t}_λ denotes the tangent at the fiber tip.

The enrichment function for the strain discontinuity across the fiber is expressed in terms of the level set functions by equation (16). The function is smooth and nonzero everywhere in the domain except along the fiber, as illustrated in Figure 7a.

$$\psi_\alpha(\mathbf{x}) = \left[\prod_{\lambda=1}^2 H(-\phi_\lambda) \right] \phi_c(\mathbf{x}) + \sum_{\lambda=1}^2 H(\phi_\lambda) d_\lambda(\mathbf{x}) \quad (16)$$

H is the Heaviside function and $d_\lambda(\mathbf{x}) = \|\mathbf{x} - \mathbf{x}_\lambda\|$ is the distance between \mathbf{x} and the fiber tip.

The debonding enrichment was derived using the same level set functions but introduces a displacement discontinuity rather than a strain discontinuity along the fiber. The debonding enrichment function is given as

$$\Upsilon_\alpha(\mathbf{x}) = \phi_p H(r(\phi_c)) \left(\prod_{\lambda=1}^2 H(-\phi_\lambda) \right) \quad (17)$$

$r = \pm\phi_c$ is the signed distance function, defined as positive on one side of the fiber level set ϕ_c and negative on the opposite side. The shape of the debonding enrichment is controlled by ϕ_p . Pike and Oskay (2015b) derived an expression for ϕ_p as a fourth order polynomial subject to constraints that the maximum debonding along the fiber occurs at the center of the fiber and the ends of the fiber remain embedded in the matrix, i.e. complete fiber pullout does not occur. The resulting enrichment function is illustrated in Figure 7b.



Figure 8. Surface deformities can be introduced into fibers during manufacturing to improve bond performance between the fiber and matrix. Common methods include crimping (top) and twisting (bottom)

4.2 Governing Equations

The governing equations for equilibrium in the model domain Ω are given by equations (18) and (19).

$$\nabla \cdot \boldsymbol{\sigma}(\mathbf{x}) = 0; \quad \mathbf{x} \in \Omega \quad (18)$$

$$\boldsymbol{\sigma} = \mathbf{L} : \boldsymbol{\varepsilon}(\mathbf{x}) \quad (19)$$

In the above equations $\boldsymbol{\sigma}$ is the stress tensor and $\nabla(\cdot)$ is the divergence operator. The stress is related to the strain ($\boldsymbol{\varepsilon} = \nabla^s \mathbf{u}$) by the elastic moduli tensor \mathbf{L} . The displacement and traction boundary conditions are defined by equations (20) and (21), respectively.

$$\mathbf{u}(\mathbf{x}) = \tilde{\mathbf{u}}(\mathbf{x}); \quad \mathbf{x} \in \Gamma_u \quad (20)$$

$$\boldsymbol{\sigma} \cdot \mathbf{n} = \tilde{\mathbf{t}}(\mathbf{x}); \quad \mathbf{x} \in \partial\Gamma_t \quad (21)$$

The boundaries Γ_u and Γ_t denote non-overlapping regions of the domain on which $\tilde{\mathbf{u}}$ and $\tilde{\mathbf{t}}$ are prescribed, with $\partial\Omega = \Gamma_u \cup \Gamma_t$. The stress in each fiber α is assumed to be axial and proportional to the axial strain by the relation $\sigma_f^\alpha = E_f \varepsilon_f^\alpha$, where E_f is the elastic modulus of the fiber. For a fiber of length l_α and diameter d_α , with $t_\alpha/l_\alpha \rightarrow 0$, the weak form of equations (18)-(21) is expressed as

$$\int_{\Omega} \boldsymbol{\sigma} : \delta \boldsymbol{\varepsilon} d\Omega + \sum_{\alpha=1}^n t_\alpha E_f \int_{\Omega_\alpha} \varepsilon_f^\alpha \delta \varepsilon_f^\alpha d\Omega + \sum_{\alpha=1}^n \int_{\Gamma_\alpha} \mathbf{T} \cdot \delta \llbracket \mathbf{u} \rrbracket d\Gamma - \int_{\Gamma_t} \tilde{\mathbf{t}} \cdot \delta \mathbf{u} d\Gamma = 0 \quad (22)$$

Ω_α denotes the domain of fiber α and Ω_m represents the domain of the matrix. Γ_α is the interface between the matrix and fiber α . $\delta \mathbf{u}$ and $\delta \boldsymbol{\varepsilon}$ represent the test function and the gradient of the test function, respectively. \mathbf{T} is the traction resulting at the interface due to the displacement jump across the fiber, $\llbracket \mathbf{u} \rrbracket$. The traction separation relationship is included in the model using an intrinsic cohesive law with uncoupled normal and shear components. In this approach pullout test data is fit to an appropriate cohesive model. The pullout test measures the reaction force at a fiber-matrix interface as a fiber is pulled out of the matrix. Cohesive properties can be manipulated in design by coating fibers and/or introducing deformities for mechanical bonding, as shown in Figure 8. Figure 9 illustrates the effect of fiber crimping on the bond behavior for a polymeric fiber embedded in a cementitious matrix. In this work a bilinear cohesive law was used to characterize the interfacial bond. Three parameters define the idealized curve shown in Figure 9: peak cohesive strength (T_n), characteristic displacement at the peak cohesive strength (δ_n) and displacement at bond failure (δ_{max}). n denotes the normal component of the traction \mathbf{T} . For the sake of simplicity, the shear parameters are assumed to be proportional to the normal components in the initial study. A range of values are used for the cohesive parameters in the numerical studies detailed in Section 5, in order to assess the influence of the bond characteristics on the response of the composite material. Pike and Oskay (2015b) provides a complete derivation of the XFEM model used herein to measure composite response of a random FRC microstructure.

4.3 Nonlocal Damage Model

A nonlocal continuum damage model is used to capture the progressive degradation of matrix stiffness. A damage parameter w that varies between 0 (undamaged) and 1 (fully damaged) is calculated based on the weighted average of the principal strains within a radial basis. As the damage parameter increases, the stiffness of the material progressively decreases until failure. An alternative continuum damage law may be easily used if deemed suitable

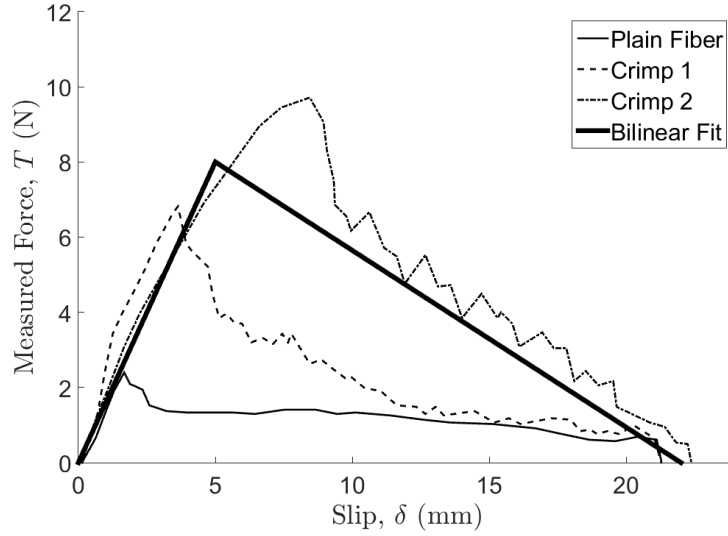


Figure 9. Example pullout test data for a ductile fiber in a cementitious matrix. The idealized bilinear cohesive law used in this manuscript is superimposed

for the matrix material of interest. At an arbitrary material point $\hat{\mathbf{x}}$ the evolution of the damage variable follows the arctangent function of equation (23).

$$w(\hat{\mathbf{x}}, t) = \frac{\arctan(a k(\hat{\mathbf{x}}, t) - b) + \arctan(b)}{\frac{\pi}{2} + \arctan(b)} \quad (23)$$

In equation (23), a and b are parameters fit to data from tests on the unreinforced matrix material. $k(\hat{\mathbf{x}}, t)$ is an increasing non-negative history dependent variable defined by equation (24).

$$k(\hat{\mathbf{x}}, t) = \max_{\tau \in [0, t]} (\langle \hat{v}(\hat{\mathbf{x}}, \tau) - v_{ini} \rangle) \quad (24)$$

\hat{v} is the nonlocal equivalent strain obtained from weighting the local equivalent strains v within a radial basis defined by $\hat{\lambda}(\mathbf{x}, \hat{\mathbf{x}})$. v_{ini} is a threshold value of equivalent strain below which damage is assumed not to progress. Equation (25) defines the local equivalent strain in two dimensions as the norm of the positive principle strains $\hat{\epsilon}_i$, which is intended to simulate stiffness degradation as cracks form in the matrix under tensile loads.

$$v(\hat{\mathbf{x}}, t) = \sqrt{\sum_{i=1}^2 \langle \hat{\epsilon}_i(\hat{\mathbf{x}}, t) \rangle^2} \quad (25)$$

The nonlocal equivalent strains are then computed using equation (26).

$$\hat{v}(\hat{\mathbf{x}}) = \frac{\int_{\Omega} \hat{\lambda}(\mathbf{x}, \hat{\mathbf{x}}) v(\mathbf{x}, t) d\mathbf{x}}{\int_{\Omega} \hat{\lambda}(\mathbf{x}, \hat{\mathbf{x}}) d\mathbf{x}} \quad (26)$$

The weights are determined using the Wendland Radial Basis Function (Wendland, 1995) given by equation (27), where l_c defines the span of the radial basis.

$$\hat{\lambda}(\mathbf{x}, \hat{\mathbf{x}}) = \left(1 - \frac{\|\mathbf{x} - \hat{\mathbf{x}}\|}{l_c}\right)^4 \left(4 \frac{\|\mathbf{x} - \hat{\mathbf{x}}\|}{l_c} + 1\right) \quad (27)$$

5 Numerical Models

The XFEM code developed by Pike et al. (2015) deals with a 2D square matrix reinforced by 1D fibers subject to uniaxial tension. A CVE domain of 50x50 mm is considered ($\lambda = 50$ mm). Square elements of 0.5 mm dimension

are used, resulting in a 10,000 element mesh. Figure 10 depicts the problem domain for a random sample. The left and bottom boundaries of the matrix are constrained against displacement in their normal directions. The right end of the domain is assigned a displacement of magnitude $u_0 = 0.1$ mm. The problem is solved using 250 fixed strain increments. Table 1 gives the properties of the matrix and fiber used in the models. While the fiber length, diameter, and cohesive properties are sampled from random distributions, as discussed later in this section, the phase material properties are assumed constant. The numerical values used are typical for a cementitious matrix material and a steel fiber.

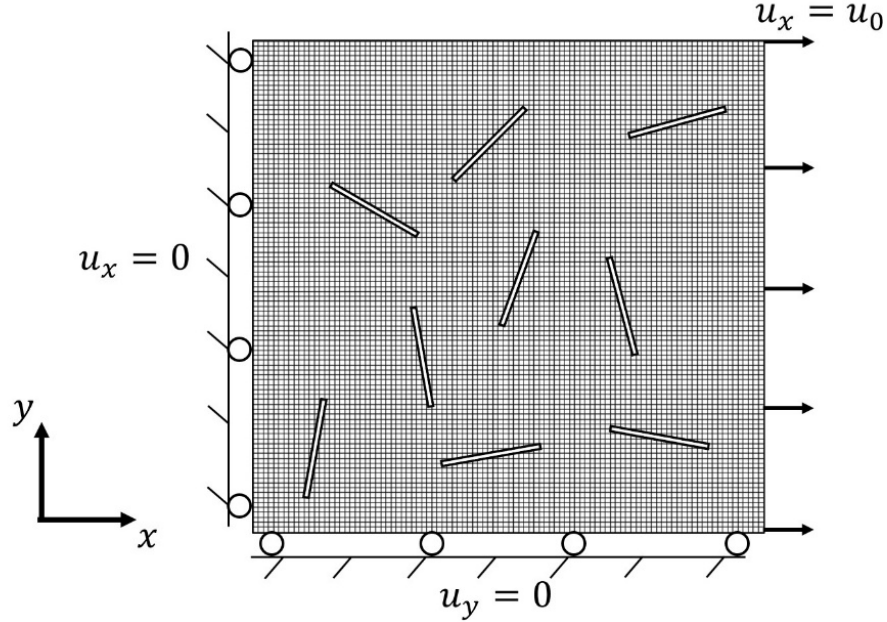


Figure 10. XFEM problem domain and boundary conditions

Table 1. Phase Material Properties

Property	Matrix	Fiber
Young's Modulus, E	14,000 MPa	207,000 MPa
Poisson's Ratio, ν	0.3	0.3
Nonlocal Damage Radius, l_c	0.75 mm	-
Nonlocal Damage Parameter, a	49,000	-
Nonlocal Damage Parameter, b	19.5	-

5.1 Sampling of Descriptor Space

Descriptors are in essence the design variables for the engineered composite material. Given some matrix and fiber material, it is necessary to identify the ideal combination of fiber length, diameter, volume content, and interfacial cohesive properties to achieve desirable inelastic response. The descriptors act as inputs to the XFEM model from which corresponding material properties are extracted. Stress vs. strain data is recorded at each increment of the analysis. Processing of the data is discussed in Section 6. Here, $n = 6$ descriptors are considered, as listed in Table 2. A point \mathbf{X} in descriptor space is defined as $\mathbf{X} = [X_1, X_2, \dots, X_{n-1}, X_n]$. \mathbf{X} is a row vector with each component representing some value of descriptor $X_j, j = 1 \dots n$. Let \mathbf{Y} denote a measured output material to be optimized, such as strain energy capacity. The constrained optimization problem is then expressed as

$$\begin{aligned}
 &\text{maximize} && \mathbf{Y} = \mathbf{H}(\mathbf{X}) \\
 &\text{subject to} && X_j \geq a_j \quad j = 1 \dots n \\
 & && X_j \leq b_j \quad j = 1 \dots n
 \end{aligned} \tag{28}$$

Here $[a_j, b_j]$ is the range of feasible design values for descriptor X_j . \mathbf{H} is the mapping from a point in input space to composite response in output space. The feasible region is defined independently in each dimension of

descriptor space by the bounds listed in Table 2. In practical applications, the feasible region of values for fiber length may be defined as the range of fiber lengths available from a manufacturer, for example. In practice, cohesive properties may be customized by applying coating to fibers or introducing deformities for improved anchorage. The process for solving the optimization problem is as follows: (1) randomly generate m samples, $\mathbf{X}_i, i = 1 \dots m$ in n -dimensional descriptor space; (2) analyze random realizations of microstructure \mathbf{X}_i using the XFEM model discussed in this section to obtain material property outputs, \mathbf{Y}_i ; (3) implement Gaussian Process regression to obtain $\mathbf{H}(\mathbf{X})$ from the data; (4) identify optimal points \mathbf{X}^* that maximize the objective function.

Table 2. Descriptor Variable Ranges

Descriptor	Lower Bound (a_j)	Upper Bound (b_j)
d_f , Fiber diameter (X_1)	0.005 mm	0.1 mm
l_f , Fiber length (X_2)	5 mm	15 mm
VF , Fiber volume fraction (X_3)	.01%	1.5%
T_n , Peak normal cohesive strength (X_4)	5 MPa	15 MPa
δ_n , Characteristic normal cohesive separation (X_5)	0.000005 mm	0.0001 mm
δ_{max} , Maximum cohesive separation (X_6)	0.0002 mm	0.0005 mm

For random sampling, a probability distribution type must be selected for each input descriptor. Descriptors may be continuous or discrete, bounded or unbounded based on the physical property they represent. In this work, continuous, bounded descriptors are considered. With $f_{X_j}(x)$ representing the probability density function (PDF) for the assumed distribution of descriptor X_j , for a general continuous random variable X_j with lower bound a_j and upper bound b_j

$$f_{X_j}(x) = P(X_j = x) \quad \forall \quad x \in [a_j, b_j] \quad (29)$$

$P(X_j = x)$ represents the probability that X_j is equal to x . The corresponding cumulative distribution function (CDF) is then defined as

$$F_{X_j}(x) = \int_{a_j}^x f_{X_j}(x) dx \quad \forall \quad x \in [a_j, b_j] \quad (30)$$

The CDF is non-decreasing and varies between 0 and 1 over the domain $x \in [a_j, b_j]$. To generate random descriptor values for sample \mathbf{X}_i , a vector of independently generated random numbers, \mathbf{r}_i is constructed in the form of equation (31).

$$\mathbf{r}_i = [r_1, r_2, \dots, r_{n-1}, r_n], \quad r_j \in (0, 1), \quad j = 1 \dots n \quad (31)$$

Using the inverse CDF of each X_j , entries of \mathbf{r}_i are converted into components of the random sample point by equation (32).

$$\mathbf{X}_i = [F_{X_1}^{-1}(r_1), F_{X_2}^{-1}(r_2), \dots, F_{X_{n-1}}^{-1}(r_{n-1}), F_{X_n}^{-1}(r_n)] \quad (32)$$

In this work a uniform distribution is used for each descriptor so that the entire range of the feasible region for a descriptor can be considered with equal bias. Using a uniform distribution, the components of \mathbf{X}_i in equation (32) can be calculated as

$$F_{X_j}^{-1}(r_j) = a_j + r_j(b_j - a_j) \quad (33)$$

In order to determine a meaningful relationship between \mathbf{X} and \mathbf{Y} , it is important that the feasible region is appropriately sampled in each dimension of the descriptor space. If components of \mathbf{r}_i are obtained independently for each of the m samples, it is possible for multiple random samples to contain similar values in some dimensions. As a result, some regions of design space may be insufficiently sampled. To avoid this issue, Latin Hypercube Sampling (LHS) is implemented. LHS is a type of stratified sampling technique in which each dimension of descriptor space is subdivided into m equal intervals. Samples are generated such that only one sample will be drawn from each interval in each dimension. Figure 11 shows 10 sample points plotted in 2 dimensions to illustrate the the concept of LHS. It can be seen that no interval on either axis of any of the three plots contains multiple samples. In this study, no correlation between parameters is used in sampling the descriptor space, i.e. each descriptor is treated as an independent design variable. For this study, 50 samples were used to discretize the feasible region defined in Table 2. For each \mathbf{X}_i , p random realizations of the microstructure are tested, denoted by $\tilde{\mathbf{X}}_i^{(k)}$, $k = 1 \dots p$, to obtain the mean and variance of each output parameter at the sample point. For initial study, a value of $p = 3$ was used. Future studies will assess the statistical significance of the sample size. More realizations of each sample point should be used to reduce the observed uncertainty.

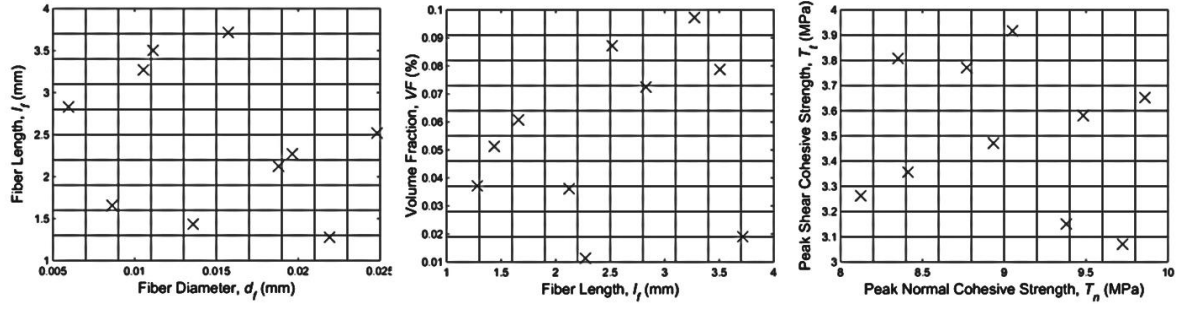


Figure 11. 2D visualization of LHS in example descriptor space with $m = 10$

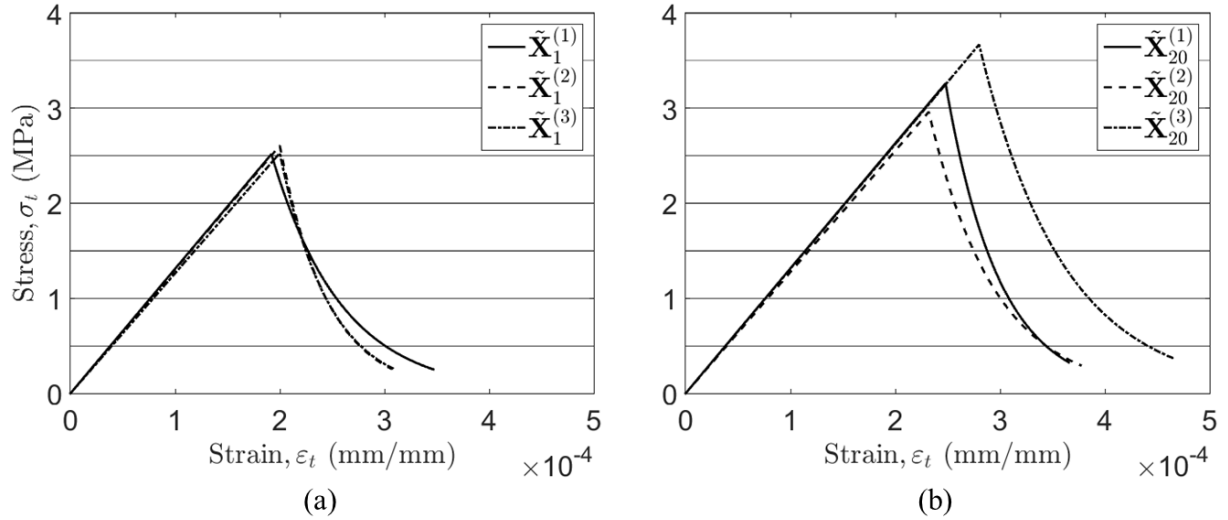


Figure 12. Sample tensile stress-strain curves for two random points in descriptor space: \mathbf{X}_1 (a) and \mathbf{X}_{20} (b)

6 Discussion of Results

Random CVE realizations $\tilde{\mathbf{X}}_i^{(k)}$, $k = 1 \dots 3$, at each point \mathbf{X}_i , $i = 1 \dots 50$ in descriptor space were modelled in tension using XFEM. Stress vs. strain data was obtained from each analysis. Figure 12 illustrates the curves obtained for each random realization at two points, \mathbf{X}_1 and \mathbf{X}_{20} . Five quantities used to characterize the material, denoted Y_q , $q = 1 \dots 5$, were measured for each sample $\tilde{\mathbf{X}}_i^{(k)}$. Table 3 identifies the measured properties. Damage in the matrix material is initiated at the fiber tips and propagates through the material to the edges of the CVE domain. As a result, higher concentrations of fibers provide additional potential damage paths, reducing the peak strength of the composite and producing more uncertainty in the post-peak response. At first glance, it can be clearly seen that \mathbf{X}_1 exhibits lower peak tensile strength and a smaller strain to failure than \mathbf{X}_{20} . The response of each realization of \mathbf{X}_1 appears nearly identical in the elastic range, with slightly increased variation being observed in the post-peak response. In contrast, realizations of \mathbf{X}_{20} show greater uncertainty in both pre- and post-peak response.

In order to quantify the uncertainty at each point \mathbf{X}_i , second order statistical information for each Y_q was obtained at each sample point in the descriptor space. The coefficient of variation (CV) of property Y_q at sample point \mathbf{X}_i observed from random realizations $\tilde{\mathbf{X}}_i^{(k)}$ is defined as

$$CV_{\mathbf{X}_i}(Y_q) = \frac{\bar{\sigma}_{Y_q}^{(i)}}{\bar{\mu}_{Y_q}^{(i)}} \quad (34)$$

$\bar{\mu}_{Y_q}^{(i)}$ and $\bar{\sigma}_{Y_q}^{(i)}$ represent the sample mean and standard deviation of Y_q observed at point \mathbf{X}_i in population $\{\tilde{\mathbf{X}}_i^{(k)}\}_{k=1}^3$. The CV compares the variability of the property to the magnitude of the expected value of the property, providing a normalized, dimensionless measure of uncertainty. Figure 13 shows the averages of computed within-cluster CV values for each material property. The average measured CV of peak tensile stress was 0.049. The lowest average CV was observed in ε_i , with a value of 0.047. The properties corresponding to the elastic region of the response

Table 3. Composite parameters measured in each numerical simulation

Identifier (Y_q)	Material Property	Description
Y_1	σ_i	Peak tensile stress
Y_2	ε_i	Tensile strain at peak stress
Y_3	ε_f	Strain at failure of composite
Y_4	G^r	Modulus of resilience
Y_5	G^t	Modulus of toughness

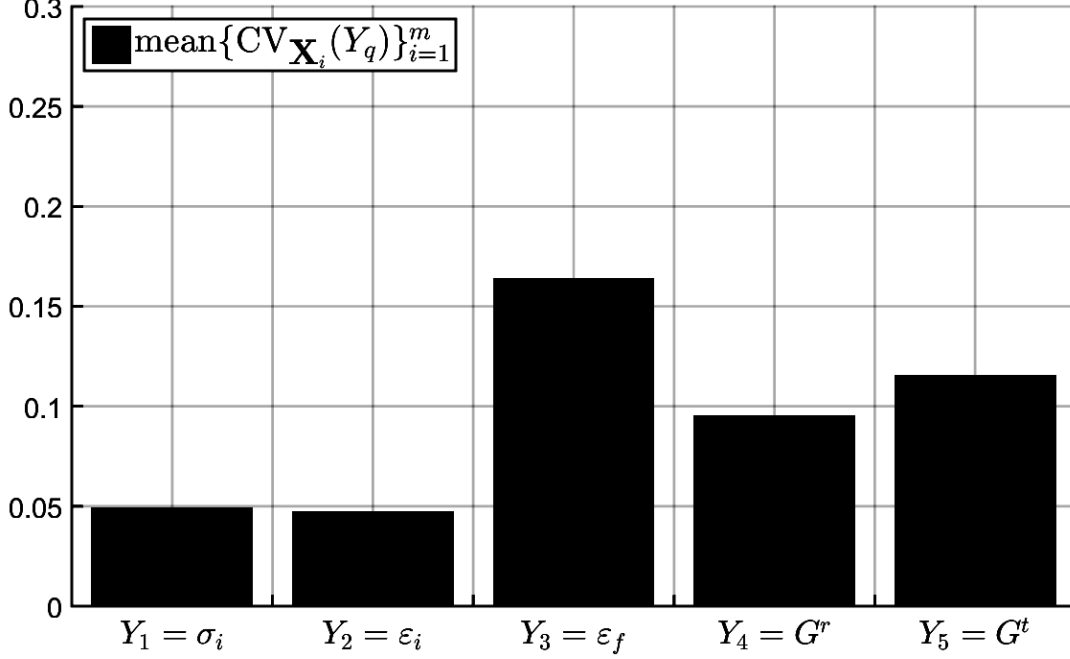


Figure 13. Average coefficient of variation for measured composite response parameters

exhibit very low uncertainty, while the highest uncertainty is observed in the modulus of toughness (0.115) and failure strain (0.164). The elastic response of the composite is largely controlled by the matrix material, while inelastic response depends on the interaction of fibers. It follows that more uncertainty arises in characterizing the post-peak response due to the randomness of the fiber locations within the problem domain.

6.1 Characterization and Prediction of Composite Properties

While clear differences may be observed in the curves obtained for \mathbf{X}_1 and \mathbf{X}_{20} (Figure 12), the complex relationship between descriptor variables and composite properties cannot be obtained by directly comparing output quantities, because each sample is characterized by a point in the six-dimensional space. Each of the six components is assumed to have some influence on the measured material properties. Gaussian process regression is implemented in order to model the function $\mathbf{Y} = \mathbf{H}(\mathbf{X})$ presented in Section 5. Rasmussen and Williams (2006) explains GP in detail and provides algorithmic approaches to regression and prediction using the method. GP can be easily implemented in Matlab and Octave using the freely available GPML Toolbox developed by Rasmussen. This section provides a brief overview of GP, focusing primarily on how the concepts can be applied to FRC characterization and property prediction.

A GP is a collection of random variables with joint Gaussian distributions defined by its mean and covariance functions, similar to a multivariate Gaussian distribution. The expression for the random function $\mathbf{H}(\mathbf{X})$ assumed to relate descriptor variables to output quantities is given in equation (35).

$$\mathbf{H}(\mathbf{X}, \boldsymbol{\omega}) \sim \text{GP} \left(m(\mathbf{X}, \boldsymbol{\omega}_m), k(\mathbf{X}, \mathbf{X}', \boldsymbol{\omega}_k) \right) \quad (35)$$

Here, $m(\mathbf{X}, \boldsymbol{\omega}_m)$ and $k(\mathbf{X}, \mathbf{X}', \boldsymbol{\omega}_k)$ represent the prior mean and covariance functions with parameters $\boldsymbol{\omega}_m$ and $\boldsymbol{\omega}_k$, respectively. Information about the expected value of $\mathbf{H}(\mathbf{X})$ is unknown, so a zero-mean function is assumed

Table 4. Descriptor values of four random test points

Point	d_f (mm)	l_f (mm)	VF (%)	T_n (MPa)	δ_n (mm)	δ_{max} (mm)
\mathbf{X}_1	0.079	7.167	0.975	9.402	0.00007	0.00024
\mathbf{X}_2	0.043	7.667	1.281	7.187	0.00002	0.00050
\mathbf{X}_3	0.094	5.421	0.695	14.812	0.00008	0.00030
\mathbf{X}_4	0.065	11.697	0.838	8.796	0.00001	0.00033

Table 5. Error magnitude for each Y_q at test points

Point	σ_i Error (%)	ε_i Error (%)	ε_f Error (%)	G^r Error (%)	G^t Error (%)
\mathbf{X}_1	1.90	1.28	0.22	1.11	0.61
\mathbf{X}_2	4.55	4.91	3.37	8.68	1.53
\mathbf{X}_3	4.64	6.99	1.42	10.63	4.05
\mathbf{X}_4	4.32	1.36	5.60	4.46	5.35
Average	3.85	3.64	2.65	6.22	2.89

for the prior value allowing the function to be defined entirely by second-order statistics. The covariance function governs the manner in which the value of $\mathbf{H}(\mathbf{X}, \boldsymbol{\omega})$ changes throughout descriptor space. The squared exponential covariance function is commonly used in GP regression for its simplicity and flexibility. The function takes the form

$$k(\mathbf{X}, \mathbf{X}') = \sigma_f^2 \exp\left(-\frac{1}{2l^2}(\mathbf{X} - \mathbf{X}')^T(\mathbf{X} - \mathbf{X}')\right) \quad (36)$$

where σ_f is a scaling parameter and l is the characteristic length scale parameter. The squared exponential covariance function provides that for two points \mathbf{X} and \mathbf{X}' close together in space there is a high likelihood that the function will return similar output values at each point, with the likelihood decreasing exponentially as the distance between the points increases. The characteristic length influences the rate of the exponential decay. However, the descriptor variables differ significantly in magnitude, so it is not reasonable to assume a common characteristic length scale for all dimensions. In this work, the following anisotropic equivalent of the squared exponential covariance function is preferred

$$k(\mathbf{X}, \mathbf{X}') = \sigma_f^2 \exp\left(-\frac{1}{2}(\mathbf{X} - \mathbf{X}')^T \boldsymbol{\Lambda}^{-2}(\mathbf{X} - \mathbf{X}')\right) \quad (37)$$

where $\boldsymbol{\Lambda}$ is an $n \times n$ diagonal matrix of characteristic correlation length values in each dimension of descriptor space. The parameters of the covariance function are determined such that the marginal likelihood is maximized, that is, the probability of obtaining data \mathbf{Y} from input \mathbf{X} using model $\mathbf{H}(\mathbf{X}, \boldsymbol{\omega})$ is optimal. In this work GP is used to regress each Y_q independently. Future studies will address the correlation of output variables.

To determine the accuracy of the GP in predicting each Y_q , 10 training points and 4 test points were randomly selected from the 50 points tested. Table 4 lists the descriptor values characterizing each test point. The training points were used to determine the model parameters $\boldsymbol{\omega}_k$. Using the trained GP, output values were predicted for each test point. The error calculated between the GP predictions and the measured outputs from the XFEM models at the test points is given in Table 5. The largest error was observed in predicting the modulus of resilience at point \mathbf{X}_3 , with a value of 10.63%. At \mathbf{X}_1 , however, the modulus of resilience was predicted with only 1.11% error. With the exception of G^r , the GP predicted each output within 7% error at each of the four test points, with an average error of less than 4% for each output.

Figure 14 illustrates the accuracy of the GP in predicting the composite properties at the test points. It can be seen that there is only one Y_q associated with each \mathbf{X}_i , which follows from the choice of LHS as the sampling method. LHS was used in this study to cover the extent of descriptor space in the most efficient manner possible. Future studies will assess the sensitivity of the model with respect to each descriptor variable by using additional sample points, as well as testing of additional realizations of each sample point to reduce the variance of the output quantities. As mentioned in Section 2, the use of a sequential multiscale modelling framework allows for the continuous development of a mesoscale model database. The GP may be easily retrained as data from additional samples is made available.

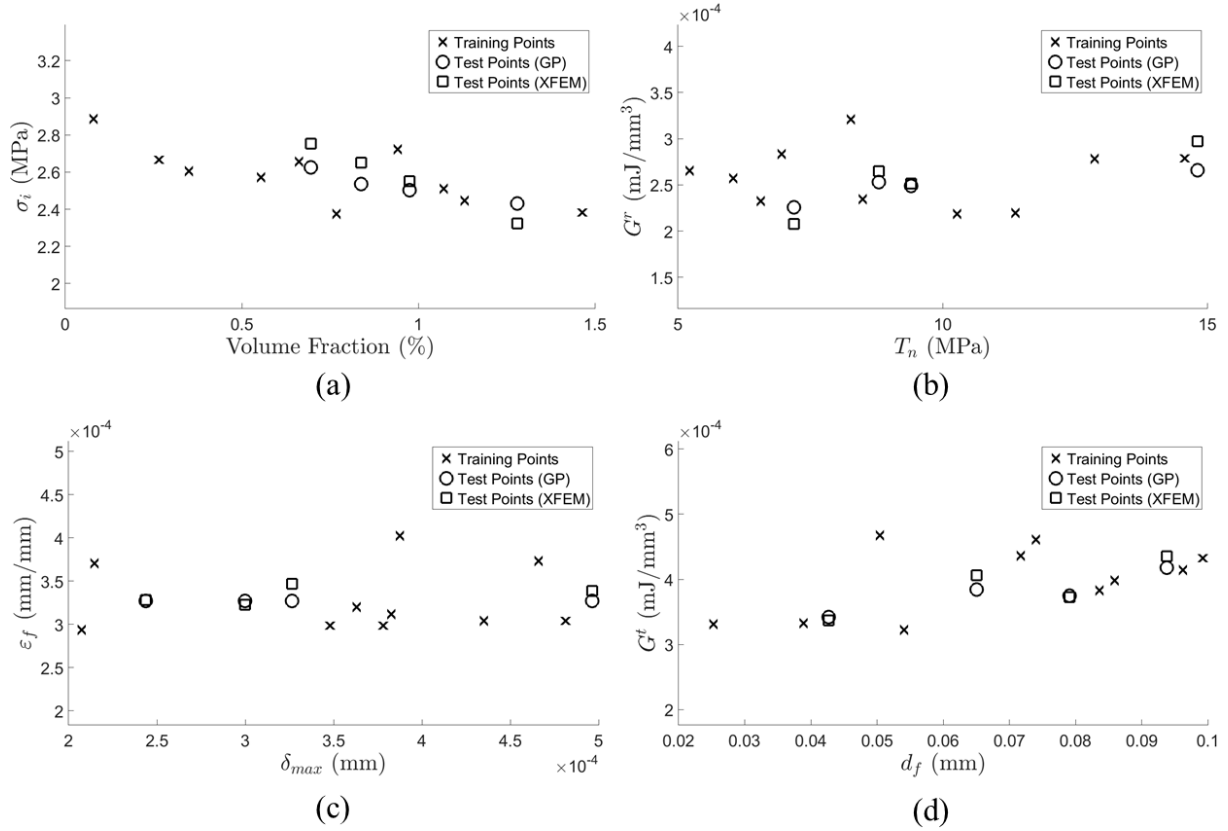


Figure 14. GP prediction accuracy at test points visualized with respect to descriptor variables: (a) σ_i vs. volume fraction; (b) G^r vs. T_n ; (c) ε_f vs. δ_{max} ; and (d) G^t vs. d_f

7 Conclusion

A sequential multiscale model for random short-fiber reinforced composites is presented. The presence of random fibers in the matrix significantly influences the tensile response of the composite material. For certain design applications, it is desirable to optimize tensile response parameters such as strain energy capacity and ductility. In Performance Based Optimal Design, microstructure characteristics including fiber dimensions, volume content, and fiber-matrix interfacial bond properties are selected as design variables influencing the response of the composite at the structural scale. The Concrete Damage Plasticity model is identified as a suitable material model for the homogenized inelastic response of FRC. In order to determine composite material properties for the CDP model, a series of analyses are performed on the mesoscale to quantify the effect of random fiber distributions. Latin Hypercube Sampling is used to draw random sample points from the feasible region of a 6-dimensional descriptor space. XFEM is used for the mesoscale simulations due to its ability to efficiently model random fiber response. The variation observed in inelastic composite properties among random realizations of each sample point is relatively large compared to the elastic properties and should be improved upon using additional samples for improved accuracy in characterization. The relationship between descriptors and composite material properties is modelled as a stochastic process. The GP model performs well in predicting composite properties.

Future work will focus on homogenization and reliability studies of macroscale composite designs using the CDP model. The mesoscale database will continue to be expanded using additional sample points in descriptor space. The effect of sample size on convergence of measured properties at a point in descriptor space will be assessed, as well as the effect of CVE size. In this work, the effect of changing fiber geometry, composition, and interface properties for a given matrix and fiber material is considered. It may be of interest to consider different fiber and matrix materials, depending on application. Failure of the composite was defined by degradation of the load-carrying capacity in this work. Fiber plasticity and fracture should also be considered as failure modes. The definition of an optimal design is dependent upon the application of interest. For some applications it may be desirable to maximize the failure strain of the composite, whereas other applications may emphasize optimization of strain energy capacity. Future studies will address specific design problems using the method discussed herein.

References

- Belytschko, T.; Gracie, R.: A review of extended/generalized finite element methods for material modeling. *Modelling Simul. Mater. Sci. Eng.*, 17, (2009), 1–24.
- Bentur, A.; Mindess, S.: *Fibre Reinforced Cementitious Composites*. Taylor & Francis (1990).
- Clement, A.; Soize, C.; Yvonnet, J.: Computational nonlinear stochastic homogenization using nonconcurrent multiscale approach for hyperelastic heterogeneous microstructures analysis. *Int. J. Numer. Meth. Engng.*, 91, (2012), 799–824.
- Clement, A.; Soize, C.; Yvonnet, J.: Uncertainty quantification in computational stochastic multiscale analysis of nonlinear elastic materials. *Comput. Methods Appl. Mech. Engrg.*, 254, (2013), 61–82.
- Daux, C.; Moes, N.; Dolbow, J.; Sukumar, N.; Belytschko, T.: Arbitrarily branched and intersecting cracks with the extended finite element method. *International Journal for Numerical Methods in Engineering*, 48, (2000), 1741–1760.
- Ghosh, S.; Bai, J.; Raghavan, P.: Concurrent multi-level model for damage evolution in microstructurally debonding composites. *Mechanics of Materials*, 39, (2007), 241–266.
- Greene, M.; Xu, H.; Tang, S.; Chen, W.; Liu, W.: A generalized uncertainty propagation criterion from benchmark studies of microstructured material systems. *Comput. Methods Appl. Mech. Engrg.*, 254, (2013), 271–291.
- Hiriyur, B.; Waisman, H.; Deodatis, G.: Uncertainty quantification in homogenization of heterogeneous microstructures modelled by xfem. *Int. J. Numer. Meth. Engng.*, 88, (2011), 257–278.
- Jankowiak, T.; Lodygowski, T.: Identification of parameters of concrete damage plasticity model. Tech. rep., Poznan University of Technology (2005).
- Kable, P.: Multiscale framework for modeling of fracture in high performance fiber reinforced cementitious composites. *Engineering Fracture Mechanics*, 74, (2007), 194–209.
- Kanit, T.; Forest, S.; Galliet, I.; Mounory, V.; Jeulin, D.: Determination of the size of the representative volume element for random composites: statistical and numerical approach. *Int. J. of Solids and Structures*, 40, (2003), 3647–3679.
- Kastner, M.; Muller, S.; Ulbricht, V.: Xfem modelling of inelastic material behaviour and interface failure in textile-reinforced composites. *Procedia Materials Science*, 2, (2013), 43–51.
- Li, V.: Postcrack scaling relations for fiber reinforced cementitious composites. *J. Materials in Civil Engineering*, 4, 1, (1992), 41–57.
- Li, V.; Fischer, G.: Reinforced ecc - an evolution from materials to structures. In: *Proceedings of the first FIB congress*, pages 105–122 (2002).
- Lublinter, J.; Oliver, J.; Oller, S.; Onate, E.: A plastic-damage model for concrete. *Int. J. Solids and Structures*, 25, (1989), 299–326.
- Pike, M.; Hickman, M.; Oskay, C.: Interactions between multiple enrichments in extended finite element analysis of short fiber reinforced composites. *International Journal for Multiscale Computational Engineering*, 13, 6, (2015), 507–531.
- Pike, M.; Oskay, C.: Modeling random short nanofiber- and microfiber-reinforced composites using the extended finite-element method. *J. Nanomech. Micromech.*, 5, (2015a), 1–11.
- Pike, M.; Oskay, C.: Xfem modeling of short microfiber reinforced composites with cohesive interfaces. *Finite Elements in Analysis and Design*, 106, (2015b), 16–31.
- Rasmussen, C.; Williams, C.: *Gaussian Processes for Machine Learning*. MIT Press (2006).
- Savvas, D.; Stefanou, G.; Papadrakakis, M.; Deodatis, G.: Homogenization of random heterogeneous media with inclusions of arbitrary shape modeled by xfem. *Comput. Mech.*, 54, (2014), 1221–1235.
- Wendland, H.: Piecewise polynomial, positive definite and compactly supported radial functions of minimal degree. *Advances in Comp. Math*, 4, (1995), 389–396.

- Xu, H.; Greene, M.; Deng, H.; Dikin, D.; Brinson, C.; Liu, W.; Burkhart, C.; Papakonstantopoulos, G.; Poldneff, M.; Chen, W.: Stochastic reassembly strategy for managing information complexity in heterogeneous materials analysis and design. *Journal of Mechanical Design*, 135, (2013), 1–12.
- Xu, H.; Li, Y.; Brinson, C.; Chen, W.: A descriptor-based design methodology for developing heterogeneous microstructural materials system. *Journal of Mechanical Design*, 136, (2014), 1–12.
- Yuan, F.; Pagano, N.; Cai, X.: Elastic moduli of brittle matrix composites with interfacial debonding. *Int. J. Solids and Structures*, 34, (1997), 177–201.
- Zi, G.; Song, J.; Budyn, E.; Lee, S.; Belytschko, T.: A method for growing multiple cracks without remeshing and its application to fatigue crack growth. *Modelling Simul. Mater. Sci. Eng.*, 12, (2004), 901–915.

Address: PMB 351831, 2301 Vanderbilt Pl., Nashville, TN 37235-1831 USA
email: mason.a.hickman@vanderbilt.edu